GA–A23775

DYNAMICS OF THE FORMATION, SUSTAINMENT, AND DESTRUCTION OF TRANSPORT BARRIERS IN MAGNETICALLY CONTAINED FUSION PLASMAS

by
P. GOHIL

NOVEMBER 2001

GENERAL ATOMICS

DISCLAIMER

GA–A23775

DYNAMICS OF THE FORMATION, SUSTAINMENT, AND DESTRUCTION OF TRANSPORT BARRIERS IN MAGNETICALLY CONTAINED FUSION PLASMAS

by
P. GOHIL

This is a preprint of a paper to be presented at the 8th IAEA Technical Committee Meeting on H–Mode Physics and Transport Barriers, Toki, Japan September 5–7, 2001, and to be published in the *Plasma Physics and Controlled Fusion.*

Work supported by
the U.S. Department of Energy
under Contract No. DE-AC03-99ER54463

GENERAL ATOMICS PROJECT 30033
NOVEMBER 2001

ABSTRACT

The formation of transport barriers in fusion plasmas is studied through examination of mechanisms which can stabilize plasma turbulence and, thereby, reduce turbulence driven transport. These include the effects of E×B velocity shear, negative central magnetic shear and the Shafranov shift. Transport barriers formed at the plasma edge and in the plasma core are considered, as well as the formation of multiple barriers. The access conditions for barrier formation are examined, particularly by considering local conditions compared to global parameters. Processes that can destroy transport barriers, such as magnetohydrodynamic (MHD) instabilities, are described. Plasmas with high confinement and good plasma stability then require effective control of plasma profiles and transport. Efforts towards real-time control of transport barriers are described.

1. INTRODUCTION

The ability to control transport in magnetically contained fusion plasmas is an important step in achieving reactor relevant plasma conditions. Understanding the physics of the formation, sustainment and destruction of transport barriers in fusion plasmas can significantly advance efforts towards reaching this goal. The types of different transport barriers observed in fusion plasmas has increased substantially since the H–mode edge transport barrier was first discovered in ASDEX [1]. These barriers range from those located near or at the plasma edge such as the very high (VH)–mode [2], enhanced D_α (EDA) H–mode [3], and QH–mode (quiescent H–mode) [4] to internal transport barriers (ITBs), which are often characterized by various configurations of the safety factor (q) profile such as negative central shear (NCS) plasmas [5], enhanced reverse shear (ERS) plasmas [6], high β-poloidal plasmas [7], or optimized shear (OS) plasmas [8].

Multiple barriers can form in the plasma as a result of the co-existence of the edge barrier with various forms of ITBs, e.g., quiescent double barrier (QDB) plasmas in DIII–D [9], multiple barrier plasmas in JET [10], high _p H–mode and RS H–mode plasmas in JT–60U [11,12]. Also, ITBs may form for only certain combinations of ions, electrons, toroidal momentum and particle barriers in contrast to edge transport barriers (ETBs) which typically have clear and well-formed barriers for all the above quantities simultaneously. Furthermore, transport barriers can be formed using many different heating methods [e.g., neutral beam injection (NBI), electron cyclotron heating (ECH), ion cyclotron resonance heating (ICRH), lower hybrid (LH), ion Bernstein wave (IBW), Ohmic] and other means (e.g., pellet injection, applied voltages, impurity injection). Determining the common features and behavior for these different conditions provides valuable information for understanding the physics of barrier formation as well as controlling the barriers. This understanding can be obtained by determining the mechanisms responsible for suppression of turbulence-driven transport in these plasmas.

The access conditions required for barrier formation very much affect the dynamics of the barrier formation. Magnetic shear, different heating methods, power deposition profiles, momentum torque, and kinetic profiles, for example, can all influence the formation characteristics of transport barriers. This is particularly the case with ITBs, in which the radial profiles of various quantities can be critical for their formation. The large pressure gradients that can develop once the barrier is formed make the barrier susceptible to plasma magnetohydrodynamic (MHD) instabilities, which can subsequently destroy the barrier. Sustained, high performance operation with stable barriers then requires dynamic control of the barriers.

This paper examines the above issues pertaining to the formation and evolution of transport barrier (both ITBs and ETBs) in fusion plasmas. Section 2 covers the formation of edge and internal transport barriers as well as multiple barriers. Section 3 examines access conditions for barrier formation. Section 4 covers the destruction of transport barriers. Control of transport barriers is covered in Section 5.

2. FORMATION OF TRANSPORT BARRIERS

2.1. STABILIZATION OF PLASMA TURBULENCE

Inherent to barrier formation is the requirement for the reduction of fluctuation-driven transport; this is most frequently achieved by stabilizing turbulence. Such plasma turbulence can result from toroidal drift waves and MHD ballooning modes. Understanding transport barrier formation then requires determining mechanisms which can stabilize turbulent modes, such as ion temperature gradient (ITG) modes, electron temperature gradient (ETG) modes and trapped electron modes (TEMs). The stabilization mechanisms have to account for the different dynamic behaviors of the various species in the plasma.

Leading mechanisms for turbulence stabilization include: (a) stabilization of plasma turbulence by E×B flow shear nonlinear decorrelation of turbulence [13–15] or by E×B stabilization of modes [16,17]; and (b) reduction of the turbulence growth rates by the Shafranov shift (α-stabilization) [18,19] in the presence of low or negative magnetic shear, which in itself stabilizes high n MHD modes (e.g., ballooning modes). Additional ITG mode stabilization mechanisms include: fast ion dilution and impurities [20,21] and increased ratios of T_i/T_e [22]. Increased T_e/T_i is stabilizing to ETG modes. Conversely, note that ITG modes are destabilized by increasing T_e/T_i whereas ETG modes are destabilized by increasing T_i/T_e. The different turbulence mechanisms (ITG, ETG, TEM) extend over different spatial scales with ITG modes being the longest wavelength, followed by the TEM (for ITG and TEM: $k_\theta\rho \lesssim 1$ where k_θ is the poloidal wavenumber and ρ is the ion poloidal gyroradius), with the ETG modes (ETG: $k_\theta\rho > 1$) covering the shortest spatial scale lengths. E×B velocity shear is effective in stabilizing ITG and TEM modes because of the comparable growth rates of the modes [23]. However, the short wavelength high-k ETG modes should not be directly affected by E×B shear because of the much larger growth rates of ETG modes. However, ETG modes can be stabilized by electron density gradients and by the Shafranov shift for low or negative magnetic shear, although the Shafranov shift can be destabilizing for ETG modes for positive magnetic shear [24]. The influence of the different stabilization mechanisms on the turbulence modes and the subsequent effect on the transport barriers is shown in Fig. 2–1. The figure shows which turbulence mechanisms are affected by the various stabilization mechanisms. In the case of the edge transport barrier, atomic processes at the plasma edge can influence the requirements for barrier formation. Also, the figure shows that the presence of an edge transport barrier can affect the formation of ITBs, and vice versa, through changes in energy flow, differences in operational conditions and perturbations, such as ELMs. Note that these mechanisms can operate interdependently, particularly since the generation of steep gradients in the transport barriers can affect the

turbulence mechanisms as well as producing feedback loops with stabilization mechanisms which can further aid formation and sustainment of the barriers. Consequently, the barrier formation process is a very dynamic interaction of many mechanisms that has to finally satisfy the threshold requirements for the barrier. In this respect, a dynamically evolving system, close to threshold conditions, can exhibit large bifurcations resulting from relatively small changes in the drive parameters. For example, this can occur in dithering H–mode transitions in which barrier formation can increase edge gradients and, thereby, the turbulence drive resulting in a loss of the barrier, which then reforms as the turbulence drive is reduced as the gradients decrease.

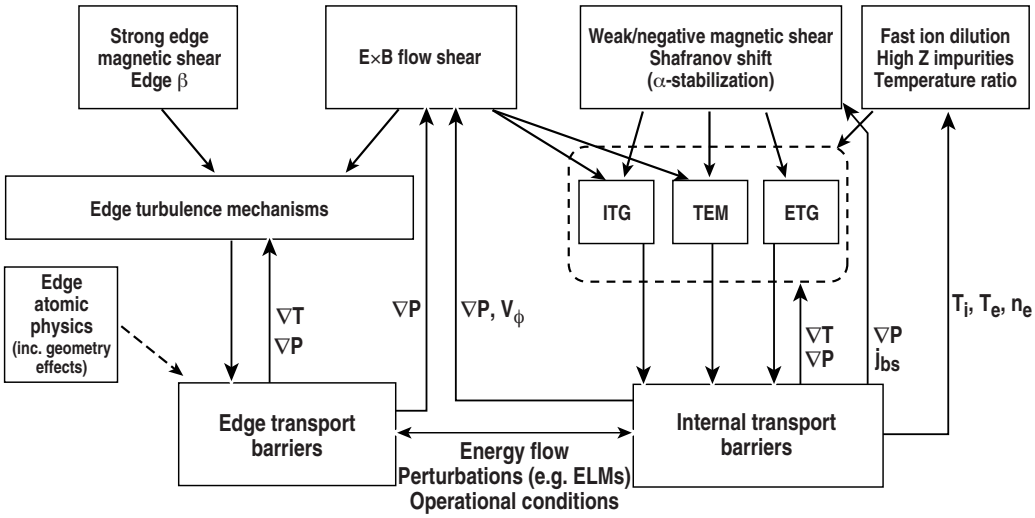

Fig. 2–1. Diagram of turbulence stabilization mechanisms, turbulence mechanisms and their relationship for transport barrier formation. Also shown are various feedback and drive parameters for the different mechanisms.

Of all the stabilization mechanisms shown in Fig. 2–1, E×B velocity shear stabilization is the only one that has been observed to apply at all locations along the plasma mirror radius, i.e., from H–mode to VH–mode to ITBs. Briefly, the nonlinear decorrelation of turbulence by E×B velocity shear [13,14] developed from early work that emphasized E_r as the stabilizing element [25,26]. For decorrelation of turbulence, the E×B shearing rate, $\omega_{E\times B}$, must be comparable to the nonlinear turbulence decorrelation rate, $\Delta\omega_D$, in the absence of E×B velocity shear [13]. This work further developed into approximate expressions for quenching unstable ITG modes [23], whereby the turbulence is completely suppressed when the E×B shearing rate, $\omega_{E\times B}$, exceeds γ_{max}, where γ_{max} is the maximum linear growth rate of the instability, determined without $\omega_{E\times B}$. An expression for the $\omega_{E\times B}$ shearing rate in the toroidal geometry is given by [27]

$$\omega_{E\times B} = \frac{RB_\theta}{B}\frac{\partial}{\partial r}\left(\frac{E_r}{RB_\theta}\right) \quad .$$

The value of the radial electric field, E_r, used in the above equation can be determined from the radial force balance equation for any plasma species, *i*, by

$$E_r = \frac{\nabla p_i}{n_i Z_i e} + v_{\phi i} B_\theta - v_{\theta i} B_\phi \quad ,$$

where n is the species density, p is the pressure, Z is the charge number, e is the electric charge, v_ϕ is the toroidal rotation, v_θ is the poloidal rotation, B_ϕ is toroidal magnetic field and B_θ is the poloidal magnetic field. Again, feedback loops involving the various terms of the force balance equation can lead to further increasing values of E_r and $\omega_{E\times B}$ so increasing and maintaining the effectiveness of E×B velocity shear stabilization. Conversely, by changing the sign and strength of the momentum terms in the force balance equation it is possible to change the $\omega_{E\times B}$ shearing rate and, hence, control the transport barrier as will be described in Section 5. Note that negative central magnetic shear and large Shafranov shifts can lead to the reduction in the growth rates [18], thus facilitating the effectiveness of the E×B flow shear.

2.2. FORMATION OF THE EDGE TRANSPORT BARRIER

The edge transport barrier in H–mode plasmas forms specifically just inside the last closed magnetic flux surface of the plasma. Typically, clear simultaneous barriers are formed for T_i, T_e and n_e. Edge transport barriers can be produced by a large variety of heating methods (NBI [1], ECH [28], LHH [29], ICRH [30], Ohmic [31]), by using an external electrode [32–34] and by pellet injection [35,36]. Despite these different formation methods, the common feature is the distinct change in the observed edge E_r at barrier formation. Because the position of the barrier is well known and localized [i.e., near the last closed flux surface (LCFS)], a large array of diagnostic systems can be optimized for fast, high spatially resolved measurements of the barrier and, in fact, good details of the barrier structure can be obtained by spatially scanning the position of the LCFS across the viewing area of diagnostic systems. Specifically, evaluation of barrier physics is very dependent on obtaining detailed measurements with adequate resolution, both spatially and temporally. For example, in DIII–D, high spatial measurements were required to determine that the width of the well-like E_r structure that formed at the plasma edge was ~1 cm and was invariant to a large range of plasma parameters [37].

In DIII–D, a long succession of detailed measurements of edge temperature and density profiles, edge E_r profiles and fluctuations have revealed important details of fluctuation behavior and the role of E_r for edge barrier formation. Key results from these studies have revealed that: (1) changes in E_r occur prior to the H–mode transition [38,39]; (2) there is a marked reduction in edge density fluctuations and fluctuation-driven particle flux coincident with barrier formation [39,40]; (3) a steep gradient in E_r forms in the region of greatest fluctuation reduction and transport barrier formation [41]; (4) $\omega_{E\times B}$ is comparable to the turbulence decorrelation rate, $\Delta\omega_D$, in

L–mode but increases significantly across the transition from L–mode to H–mode and $\omega_{E\times B}$ is significantly greater than $\Delta\omega_D$ in the H–mode [42]; and (5) there is a decrease in the radial correlation length across the H–mode transition [42]. Figure 2–2 shows the changes in E_r and fluctuations across the L–H transition in DIII–D. The above results are consistent with E×B velocity shear causing reduction in fluctuations and transport barrier formation. Clear changes in E_r have also been observed at the formation of the edge barrier in JFT–2M [43], ASDEX [44], W7–AS [45], and Compass–D [46]. More recently on JFT–2M changes in potential at the plasma edge across the L–H transition have been observed with the drop in fluctuations on fast timescales of 10–100 μs using a heavy ion beam probe (HIBP) [47]. On the H–1 heliac, clear correlation is observed between ∇E_r and the fluctuation amplitude over multiple L–H cycles [48].

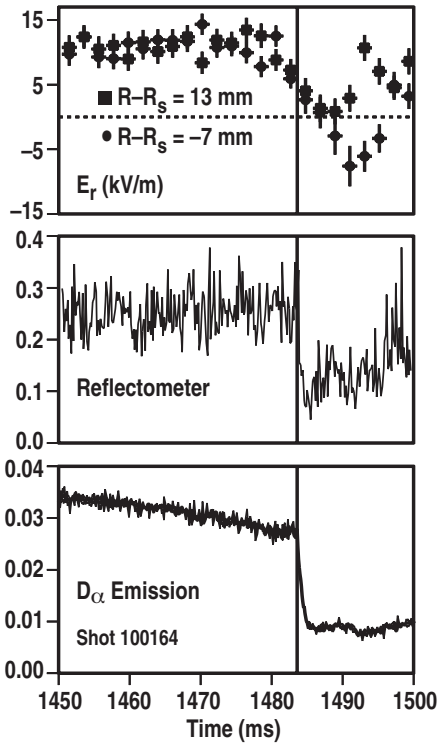

Fig. 2–2. Time histories across a L–H transition in DIII–D showing changes in (a) the radial electric field, (b) density fluctuation, and (c) divertor D_α emission. Changes in E_r are observed before the decrease in the fluctuations and the D_α signal.

The role of E×B velocity shear for barrier formation is made even clearer in experiments where H–mode transitions are directly triggered by biasing the plasma edge [32–34]. In these experiments, the edge barrier is directly formed by creating a radial electric field at the plasma edge using an electrode inserted in the plasma edge. Experiments on TEXTOR [34], show that changes in ∇E_r are correlated temporarily and spatially with changes in the electron density gradient and improvements in particle confinement. The temporal behavior of these changes is shown in Fig. 2–3 where oscillations in the bias voltage supply produced oscillations in ∇E_r

[34,49]. The oscillations in ∇E_r cause oscillations in ∇n_e with the ∇E_r oscillations leading the oscillations in ∇n_e by about 4–6 ms. The ∇E_r leading ∇n_e demonstrates that E×B shear directly affects transport.

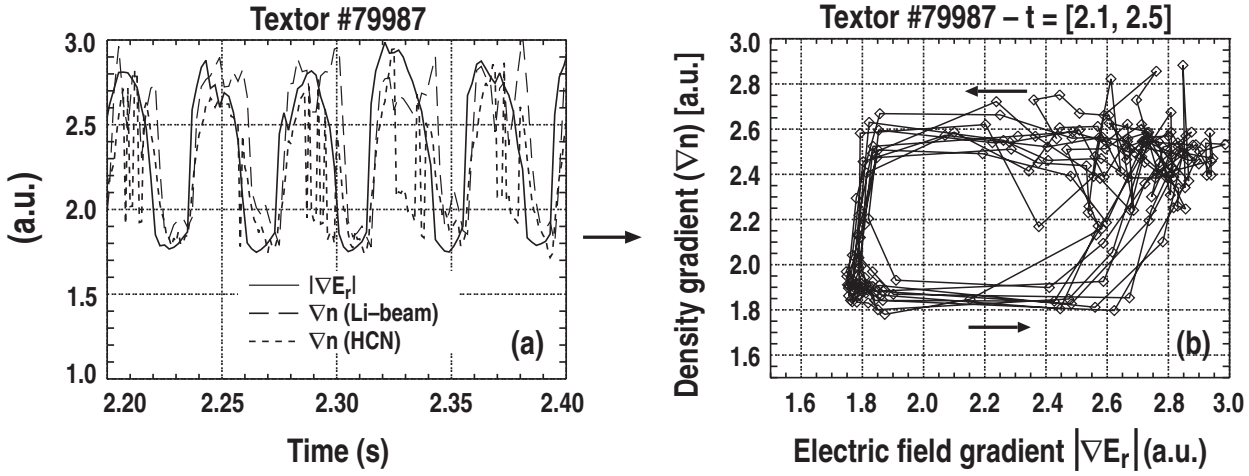

Fig. 2–3. (a) Time history of the maximum gradient of the radial electric field, ∇E_r, and the electron density gradient, ∇n_e, for a biased electrode H–mode in the TEXTOR tokamak. (b) Hysteresis diagram of ∇E_r versus ∇n_e for the data shown in (a). The time resolution of the E_r and n_e measurements are 0.04 ms for E_r, about 2 ms and 0.02 ms for the n_e measurements by the lithium beam and HCN laser systems, respectively. The direction of the arrows in (b) indicate increasing time and show that changes in ∇E_r precede changes in ∇n_e. (Results are replotted from [33], [48].)

Although the generation of sheared flow is easily understood for applied plasma biasing, the origin of the generation of sheared flows in spontaneously produced H–mode transitions (i.e., produced by heating the plasmas) has yet to be resolved. Theoretical models have proposed schemes such as neoclassical ion-orbit loss mechanisms [26], Stringer spin-up of poloidal flow [50] and shear flow driven by turbulent Reynolds' stress [51] in a nonlinear self-organized manner [52]. Results from DIII–D [53] have showed that the rotation direction of the majority ion species is inconsistent with orbit-loss mechanisms. No clear measurements of the Stringer spinup of poloidal flow have yet been made. However, recently, experiments on DIII–D [54,55] have used the nonlinear signal processing technique known as bispectral analysis to address the issue of self-organization and turbulence-generated (zonal) flow shear. Fluctuation data across the L–H transition were obtained with a reciprocating Langmuir probe and analysis of three-wave phase coherence of the potential fluctuations using the (squared) auto-bicoherence method [54]. Basically the signature of Reynold's stress driven flow shear should be seen as an increase in the coherence between different fluctuation scales. Figure 2–4 shows the total bicoherence of the ion saturation current just inside and outside the LCFS. The results indicate that three-wave coupling (bicoherence) between low and high turbulence frequencies (large and small scales) increases just before the L–H transition and before the reduction in plasma turbulence. The transition in bicoherence occurs in the region of increased E×B velocity shear at the L–H

transition and decays a few milliseconds after the L–H transition. These results are consistent with a transient Reynolds' stress driven zonal flow shear [56].

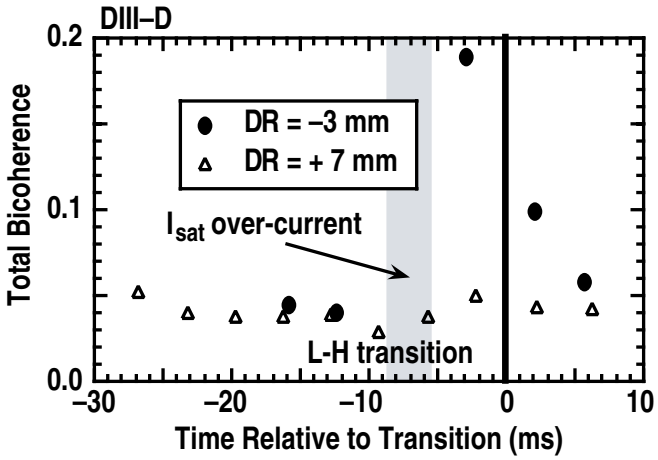

Fig. 2–4. The total bicoherence of potential fluctuations, as measured by a reciprocating Langmuir probe in DIII–D for locations inside (–3 mm) and outside (+7 mm) the separatrix across the L–H transition. The shaded region represents lack of data for the –3 mm location due to I_{sat} over-current. The data was taken over two identical shots [53].

One approach to determining the physics of the edge barrier formation is to study plasma conditions in which there are large differences in the input power requirements for the barrier formation. One such effect is the 2–3 factor change in the H–mode power threshold, P_{th}, when the direction of the ion ∇B drift is reversed with respect to the divertor X–point location [57]. Measurements of the spatially resolved edge density fluctuations in L–mode plasmas on DIII–D indicate that the poloidal group velocity of the fluctuations in L–mode change significantly when the ∇B drift direction is reversed [58]. High shear in the poloidal velocity is associated with a low P_{th} when the ∇B drift is towards the X–point and low shear in the poloidal velocity occurs for a high P_{th} when the ∇B drift is away from the X–point. The velocity shear is observed to increase with the heating power. These results indicate that shear in the edge poloidal group velocity facilitates the formation of the edge barrier and may affect the power threshold for its formation.

VH–mode plasmas on DIII–D [2] and JET [59] have improved confinement over H–mode plasmas as a result of the penetration of the edge transport barrier deeper into the plasma. Their formation results from changes in the E×B flow shear [60] over a larger region inside the plasma edge, in which density fluctuations are observed to decrease [61], as well as the local thermal diffusivities [62]. As a further example of the causal effects of the E×B velocity shear, magnetic braking experiments in VH–mode and high ℓ_i discharges in DIII–D [63–65] showed that as E×B

flow shear was reduced, there was an increase in both the amplitude of the density fluctuations and the transport rates.

H–mode edge transport barriers can suffer from large transient energy and particle losses caused by edge localized modes (ELMs). However, ELMs are useful for density and impurity control in the plasmas. ETBs can now be formed that provide good particle control, but which do not exhibit ELM activity, which (in the case of Type I ELMs [66]) can produce large peaked heat loads to the divertor surface and which can also couple to core MHD modes (e.g., neoclassical tearing modes) thereby reducing the operational beta limit [67]. Such examples of quiescent ELM-free H–mode barriers consist of the enhanced D_α (EDA) mode in C–Mod [3] and the quiescent H–mode (QH–mode) in DIII–D [4,68]. Density control in these barriers results from the increased particle transport caused by edge oscillations, defined as the quasi-coherent mode in C–Mod [69] and the edge harmonic oscillations (EHO) in DIII–D [4]. The grassy ELMing H–mode in JT–60U [70], formed at high triangularity ($\delta \sim 0.45$), high safety factor ($q_{95} \sim 6$) and high enough beta poloidal ($\beta_p \sim 1.6$) should also be included because of the dramatic change in ELM behavior at those conditions. The most recent of these regimes is the QH–mode in DIII–D (Fig. 2–5). The formation of the QH–mode requires counter-NBI at power levels above ~3.0 MW (at low current) with divertor cryopumping to lower the plasma density ($\bar{n}_e \sim 2\text{–}3 \times 10^{19}$ m^{-3}) and a large separation (~10 cm) between the plasma edge and the outer vessel wall

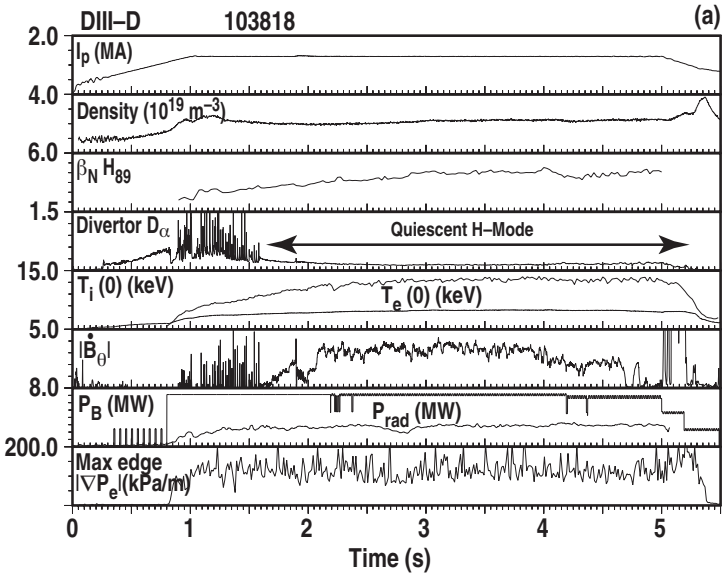

Fig. 2–5. Time histories of several plasma quantities for an ELMing H–mode plasma that transitions into a QH–mode that lasts for over 3.5 s (25 τ_E) in DIII–D (I_p = 1.3 MA, B_T = 2.0 T). The onset of the EHO is marked by the steady rise in the $\dot{B}_\theta$ signal after the ELMing phase. The edge ∇P_θ in the QH phase is the same as in the ELMing phase so indicating the good H–mode edge barrier [4].

(low toroidal field side) to apparently minimize the interaction of fast ions (resulting from the different edge ion orbits with counter-NBI) with the vessel wall. The formation of the QH–mode is marked by the onset of the EHO which is a continuous electromagnetic oscillation with multiple harmonics with toroidal mode numbers varying from 1 to 10 as measured by magnetic probes [4]. Measurements of the density fluctuations at the plasma edge indicate that the EHO peak is located at the foot of the barrier about 1 cm outside the LCFS. Density control is achieved through the EHO. The cause of the EHO is, as yet, unknown. It should be noted that measurements of the edge radial electric field, E_r, profiles indicate that QH–mode plasmas have 2–3 times deeper E_r wells inside the separatrix compared to standard ELM-free H–modes with co-NBI [71], which may have a bearing on the formation of the EHO.

2.3. FORMATION OF INTERNAL TRANSPORT BARRIERS

The formation dynamics of internal transport barriers differ from those of the edge barrier in that they are very dependent on the plasma profiles over a large region of the plasma. For example, the input power deposition profile is a critical quantity for ITB formation [72], whereas, spontaneous edge barrier formation is considered to be dependent on just the total power loss through the LCFS. Similarly, electron density and temperature profiles, momentum torque profiles, and q-profiles also all affect the evolution of ITBs. Controlling the current density profile, by heating the plasma during the current ramp (to increase the core T_e and conductivity and, hence, the current diffusion time), or by off-axis current drive, can produce regions of low or negative central magnetic shear [$s \lesssim 0$, where $s \sim (r/q)\,(dq/dr)$ is the magnetic shear], which together with the Shafranov shift can facilitate the production of ITBs through stabilization of drift wave turbulence and MHD ballooning modes [18,19]. Furthermore, elevated values of q ($q > 1$) leads to avoidance of sawteeth, which can significantly degrade or limit formation of ITBs. However, it should be noted that the presence of negative magnetic shear in itself is not sufficient for the formation of an ITB as shown in TFTR RS discharges which did not transition to the ERS phase [73]. Similarly, negative magnetic shear is not necessary for ITB formation as shown by the high β_p mode plasmas in JT–60U [7], where ion temperature and particle barriers can be formed in plasmas with positive central magnetic shear. However, negative magnetic shear appears to be important for electron ITBs as in Tore Supra [74]. Synergy between magnetic shear effects and E×B flow shear stabilization of turbulence can effectively enhance the degree of overall stabilization.

Typically, ITBs form first in the plasma core and then expand radially outwards (e.g., JT–60U [75], DIII–D [76], and JET [8]). This behavior is in agreement with theoretical predictions of barrier propagation [77] in which the core fluctuations are stabilized in the plasma core first, as a result of the lowered instability growth rates there due to magnetic shear effects and the Shafranov shift. Subsequently, radial expansion of the barrier then follows until the local stabilization by E×B velocity shear cannot overcome the radially increasing instability growth

rate. This would explain the importance of maximizing the input power near the plasma core in order to increase plasma gradients and rotation there to drive higher E×B velocity shear. In a similar but opposite manner, the ITBs contract radially inwards on reduction of input power as the E×B velocity shear at the barrier's edge decreases below the instability growth rates.

The formation of ITBs are marked by a sharp decrease in plasma fluctuations similar to that observed for the edge barriers. In TFTR, the bifurcation to the improved core confinement Type I ERS regime [6] is marked by a fast reduction in core density fluctuations [78]. In DIII–D, steps in the barrier expansion are correlated with clear transient reduction in fluctuations [79]. This bursting nature of the fluctuation reductions is consistent with modeling of the barrier dynamics [80] in which the turbulence is locally reduced transiently in the region of barrier expansion. Figure 2–6 shows reflectometry measurements on JET indicating reduction in density fluctuations over a large frequency range as the barrier forms and expands [81].

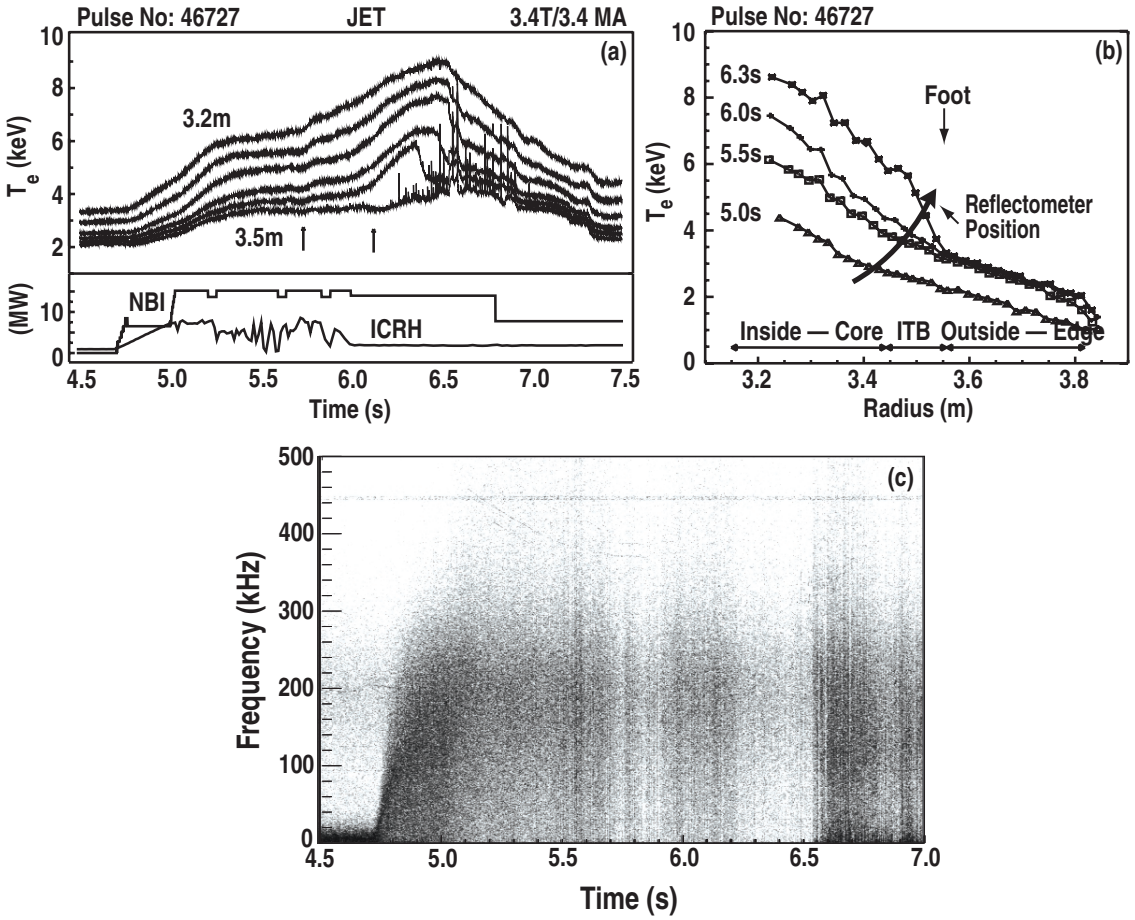

Fig. 2–6. (a) Time histories of the ECE electron temperature at several radial locations and the neutral beam and ICRF heating waveforms. (b) Radial profiles of the electron temperature during the ITB development. Also shown is the movement of the radial location of the reflectometer measurement. (c) Spectrogram (log intensity) of density fluctuations for 92 GHz core reflectometer channel. A weak barrier is produced at the first arrow in (a) followed by the formation of a strong barrier at the second arrow [80].

Spatial and temporal correlation has been observed between increased E×B velocity shear and reduction in core turbulence and subsequent improvement in core transport (e.g., in DIII–D [79,82–85] in TFTR [73,78], in JET [81]). Evaluation of the E×B shearing rate indicate that $\omega_{E\times B}$ is comparable to γ_{max} before the barrier formation and is higher after formation (e.g., in DIII–D [79,82,85], in TFTR [73,78], in JET [86,87]). This correlation is even clearer in fast bifurcations in the core transport as observed in Type I ERS transition in TFTR [73,78] in which the bifurcation to the improved core confinement enhanced reverse shear (ERS) regime in TFTR [6] is marked by a fast reduction in core density fluctuation [78] when $\omega_{E\times B}$ is comparable to γ_{max} in the plasma core. $\omega_{E\times B}$ is then further increased by positive feedback from the increasing pressure gradient. Increase in the $\omega_{E\times B}$ shearing rate comparable to γ_{max} have also been observed in ITBs formed by impurity injection in DIII–D [88,89].

Modeling of dynamic behavior of the ITB also shows the importance of E×B velocity shear. In the case of DIII–D, barriers have been observed to form and expand in a stepwise manner temporally with transitions observed in measurements of T_i, T_e and v_ϕ. A transport model (GLF23) [90] based on a gyro-Landau-fluid treatment of drift-wave ballooning modes [91] and which includes E×B flow shear, Shafranov shift and magnetic shear effects, was used to examine the evolution of the profiles. The model used 3–D gyrokinetic stability calculations for the linear growth rates and 3–D nonlinear gyro-Landau-fluid simulations to determine the saturation levels. The temperature and toroidal rotation were evolved while self-consistently computing the effects of E×B flow shear stabilization. The GLF23 model predictions indicated that the barrier would form and expand in a stepwise manner, consistent with the experimental observations. In the model simulations, the steps are transport bifurcations resulting directly from local E×B flow shear stabilization and, more specifically, from competition between the diamagnetic and toroidal rotation contributions to the E×B flow shear. Note that these steps are not observed for ITBs formed in DIII–D discharges heated with neutral beam injection counter to the plasma current direction (counter-NBI) because the diamagnetic and toroidal rotation terms then become additive and competition between the terms is removed. Also, these steps are not present with co-NBI at high initial input power levels much greater than the threshold power, in which case, the pressure gradient in the transport barrier forms rapidly and increases until the discharge disrupts at the beta limit.

Analysis of JET discharges in which both ion and electron ITBs were present, indicates that the formation, evolution and radial location of the ion ITBs can be explained by E×B shear flow stabilization of ITG-driven electrostatic turbulence [86,87]. The inclusion of magnetic shear effects further lowered the linear growth rates [90] and provided good agreement between simulation and experimental results. Note that even weak magnetic shear effects can aid in reducing plasma turbulence [92,93].

A further example of the causal effects of E×B velocity shear on turbulence suppression is obtained from experiments on TFTR, in which clear changes in the density fluctuations and

particle diffusivity where observed after the E×B shearing rate was deliberately altered in the sustained phase (postlude) of ERS plasmas [73]. The E×B shearing rate was changed by altering the mix of co-injected and counter-injected neutral beams (and, thereby, the toroidal rotation) at constant input power. In fact, the sign and strength of the toroidal rotation was effectively altered so that E_r went from pressure gradient driven to being dominated by the toroidal rotation. Subsequently, the E×B shearing rate initially decreased and then increased causing a subsequent increase in the transport followed by reduction in transport in direct response to the E×B shearing rate [73].

In certain devices where magnetic shear effects on growth rates are less evident, the direct role of E_r on fluctuation reduction is more apparent. For example, on the compact helical system (CHS) device, an electron ITB (e-ITB) is formed in an ECH heated plasma as a result of a bifurcation in the electric potential profiles (and, hence, E_r) as measured by an HIBP [94]. This bifurcation results in a region of strong E_r shear. About 50% reduction in the density fluctuation is observed at the location of maximum ∇E_r, which also marks the location of the e-ITB.

A better understanding is required of trigger mechanisms that cause the initial increase in sheared perpendicular rotation for fast bifurcations in the plasma core. For example, an analysis model based on turbulent viscous stress and neoclassical viscous damping of the poloidal velocity [95] has been used to explain the precursors in the impurity poloidal rotation observed in TFTR prior to the transition to ERS plasmas. Observations on ASDEX Upgrade indicate that ITBs form after the onset of (m,n) = (1,1) and (m,n) = (2,1) fishbone oscillations [96,97]. The ITBs then exhibit further increase in confinement with increasing frequency of the fishbone activity. It is suggested that interaction between the fishbones and the fast particles from neutral beam injection leads to a redistribution of the resonant fast particles causing a net current of fast ions outwards. The resulting return current in the bulk plasma (and, hence, electric field) then leads to a sheared poloidal plasma rotation, which in turn, results in suppression of the plasma turbulence. Numerical nonlinear simulations indicate that the total sheared flow generated by the fishbones can become comparable to the linear growth rates of the ITG modes if the time interval between fishbones is smaller than the timescale for neoclassical poloidal velocity damping [98].

Simultaneous ITBs in the n_e, T_e, and T_i have been observed in DIII-D [99], JT-60U [75], JET [100] and ASDEX Upgrade [101], but often the ITB is obtained in only one or two of the transport channels. The most pervasive ITBs in many devices are formed as a result of reduction in the ion thermal transport (i.e., ion ITBs), often to neoclassical levels. Significant reduction in the electron thermal transport is often not observed and the electron transport remains higher than neoclassical transport. Conversely, in some devices with predominantly electron heating, strong electron ITBs are formed (e.g., in Tore Supra with LHCD [74,102] and ICRH [103], in JET with LHCD [104], in DIII-D with ECH [105], in ASDEX Upgrade with counter-ECCD [101], in FTU with ECH [106], in TCV with counter-ECCD [107] in RTP with ECH [108]. Also, ITBs have been formed with IBW in PBX-M [109] and FTU [110] and by ICRH in C-Mod

[111]. Not surprisingly, the type of ITBs formed is dependent on which turbulence suppression mechanisms are effective against the turbulence present in the plasma. E×B flow shear stabilization is very effective against low-k (long wavelength) ITG fluctuations [90], which can strongly affect ion thermal and angular momentum transport in plasmas. This is particularly favorable for ion ITB formation with predominantly ion heating with neutral beams in which the Shafranov shift (α-stabilization) combined with high values of T_i/T_e (which stabilize ITG and TEM modes) facilitate the affect of E×B flow shear. In the case of electron ITBs, reduction of high-k (short wavelength) electron temperature gradient (ETG) fluctuations may be required in addition to reduction in ITG turbulence. However, E×B flow shear is considered to be less effective against ETG fluctuations because of the smaller spatial scale length and higher growth rates [112]. This is especially the case in the absence of any externally applied momentum torque to increase E×B flow shear [102-108].

Results from many devices indicate that the presence of negative central shear is an important factor in the formation of electron ITBs. In JT-60U, electron ITBs are readily formed in reverse shear plasmas [75], whereas they are only observed in the weak positive magnetic shear (high-β_p H-mode) plasmas at high triangularity [11]. In ASDEX Upgrade, an electron ITB is formed in the presence of negative central shear, although the foot of the ITB is close to the region of zero magnetic shear [101]. In Tore Supra, off-axis LHCD is used to produce ITBs in the so-called hot core LH enhanced performance mode (LHEP mode) [74,102]. The application of off-axis LHCD produces various configurations of central magnetic shear from monotonic positive shear, to weak (zero) shear and negative shear. Electron ITBs are only produced with weak to negative magnetic shear and increasingly large reductions in central χ_e are exhibited as the central magnetic shear becomes more negative [74,102] (Fig. 2–7). In JET, strong electron ITBs are produced with LHCD in the presence of highly negative central magnetic shear [104].

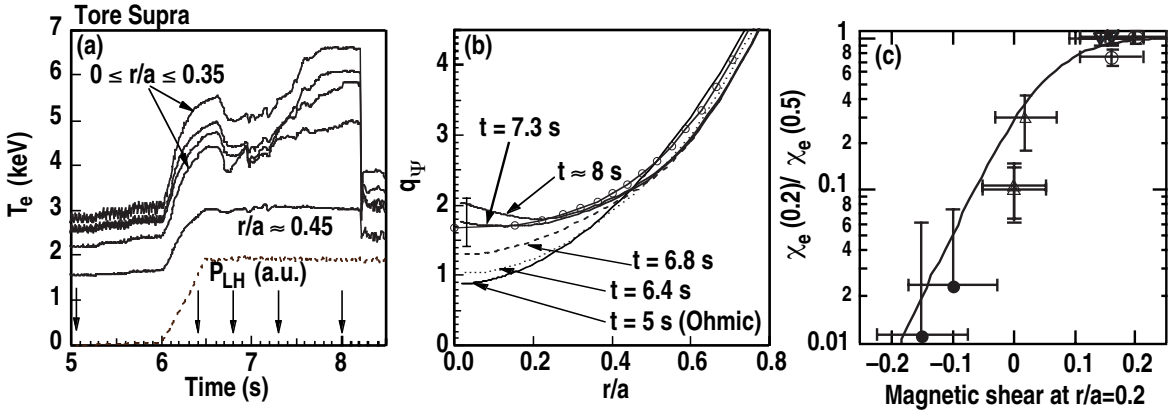

Fig. 2–7. (a) Time histories of the electron temperature (ECE) at various radial locations with the application of off-axis LH in Tore Supra (P_{LH} = 4 MW). A spontaneous transition to the LHEP mode occurs at about 7.3 s. (b) Simulated q-profile evolution using hard x-ray bremsstrahlung profiles showing the q-profile becoming flatter with time with LH. The spontaneous transition occurs when the magnetic shear in the plasma core is reduced close to zero. (c) The ratio of the electron diffusivity at r/a = 0.2 and r/a = 0.5 versus the magnetic shear at r/a = 0.2 for various non-inductive LHCD regimes [73,99].

No ion ITBs are produced and $T_e/T_i \simeq 5$ during the LHCD. In these JET discharges, the electron ITBs persist for the duration of the applied LHCD and the foot of the e-ITB is located near the region of high negative shear and well inboard of the location of q_{min}. When ICRH was applied to replace the LHCD after 2 s, the central magnetic shear became less negative and eventually became zero. During this time, the e-ITB weakens and then disappears. Therefore, in JET, there appears to be a correlation between the duration of the e-ITB and the sustained negative central shear.

In DIII-D, electron ITBs have been formed with high power NBI into strong NCS plasmas [113] and by off-axis ECH [105]. With dominant electron heating using ECH, strong e-ITBs form with $T_e/T_i \approx 10$ [105]. In these plasmas, the experimentally measured electron temperature gradient ∇T_e at the transport barrier [105,113] is very close to the calculated theoretical critical temperature gradient, ∇T_e^{crit}, for the ETG mode instability as calculated using the gyrokinetic linear stability (GKS) code [114], and is consistent with ETG modes dominating electron thermal transport at the transport barrier. Modeling of these discharges using the GKS code [114] and the GLF23 code [90] showed that α-stabilization is needed to reduce the turbulence growth rates since, without α-stabilization, the calculated ∇T_e^{crit} would be significantly lower than the experimentally measured ∇T_e [105,113]. Also, simulations of T_e profiles, starting with experimental profiles after the e-ITB has formed, indicates that the e-ITBs are only maintained in the calculated solution if α-stabilization is included [105], as shown in Fig. 2–8. This effect, however, is not noted in all devices. For example, electron ITBs are formed in Tore Supra at low beta and lower q values [74], where the effect of the Shafranov shift is small.

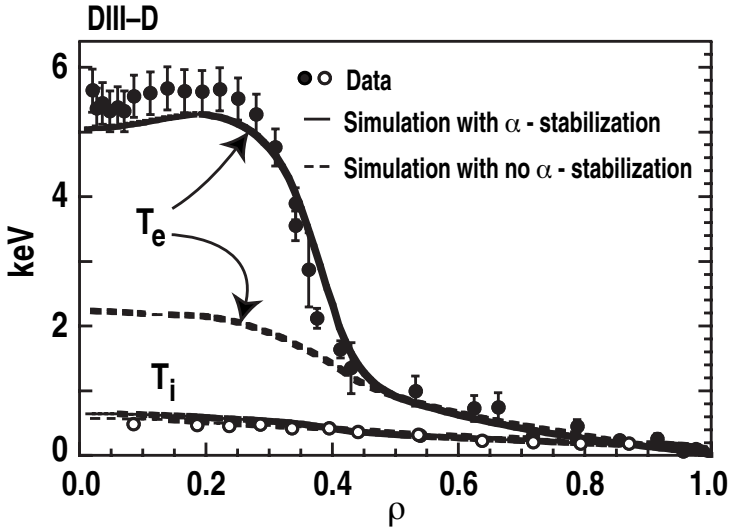

Fig. 2–8. Electron and ion temperature profiles for an electron ITB produced with ECH in DIII–D. The results of simulations with the GLF23 model with and without α-stabilization are shown by the solid and dashed lines, respectively [102].

In ASDEX Upgrade, calculation of the ITG turbulence growth rates using the GLF23 model in discharges with significant ECH, indicate that the inclusion of the Shafranov shift leads to an overall reduction of the ITG growth rates, comparable to the E×B shearing rate [Fig. 2–9(a,b)] despite the destabilizing effect of the increased ratio of T_e/T_i on the ITG modes [115]. These results indicate that the Shafranov shift can facilitate the effectiveness of E×B flow shear stabilization.

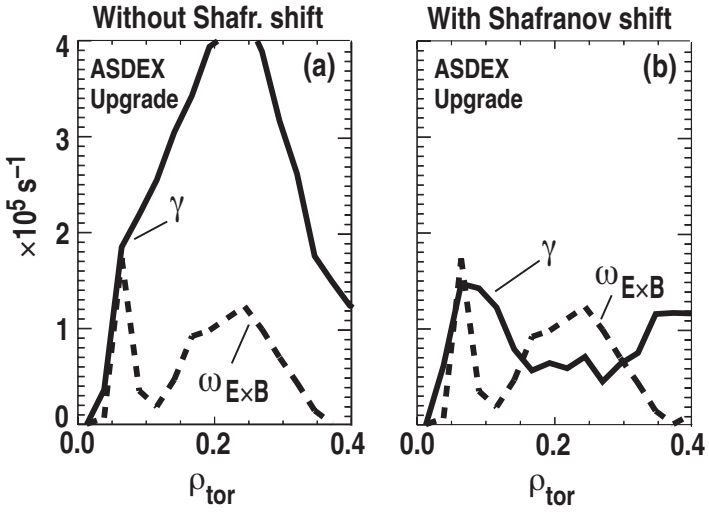

Fig. 2–9. (a) E×B shearing rate and ITB growth rate profiles for a discharge with both ion and electron ITBs produced with NBI and ECH in ASDEX Upgrade. The growth rate is obtained from the GLF23 model without including the effects of the Shafranov shift. (b) E×B shearing rate and growth rate profiles for same discharge as (a), but now including the effects of the Shafranov shift in the model [112].

The presence of negative central shear, however, is not essential for electron ITBs in some devices, as observed in TUMAN–3M, where an electron ITB was formed in an Ohmic H–mode plasma in the presence of a monotonic central magnetic shear [116], and in High-β_p H–mode plasmas at high triangularity in JT–60U, which have weak positive shear [11]. Note that the electron transport is often higher than neoclassical transport even in electron ITBs.

Apart from ITB formation being affected by the radial dependence of the q-profile, the barrier formation and evolution can also be affected by the presence of surfaces with q = integer or low-order rational values and by the radial location of q_{min}. (Conversely, deterioration of well-formed ITBs can also occur when q crosses integer values as will be discussed in Section 5). For example, in TFTR an ITB was formed in Type II ERS discharges when q_{min} was close to 2 [117]. In RTP, the high confinement regime observed in reversed shear plasmas was only formed when q_{min} decreased below 3 [118]. In JT–60U high-β_p discharges, the ITB is often observed to form at about the location of q = 3 surface [119]. Again in JT–60U, ITBs produced

by pellet injection are located at the q = 1 surface [120], whereas in the reverse shear plasmas, the ITB forms in the plasma core and expands out to the radial location of q_{min}, $\rho_{q_{min}}$, and then tracks just inside $\rho_{q_{min}}$ [75]. In JET optimized shear discharges with near flat central current profiles, strong ITBs are formed when target plasmas have central q values, q_0 close to 2 [121] or close to 1 [122] although barriers are sometimes formed when q_0 is close to 3 [123]. Weaker ITBs are formed for the same input power for non-optimum values of q_0 (i.e., $q_0 \neq 2$). However, the sensitivity of ITB formation (and subsequent plasma performance) to the target $q_0 = 2$ surface is observed for input powers close to the threshold power for ITB formation. At higher input powers, ITB formation and plasma performance becomes increasingly less sensitive to the target q_0 value. This indicates that sensitivity of ITB formation to integer q-surfaces may be a consequence of operating at input powers close to the threshold power for ITB formation. It also suggests that the power needed to form an ITB depends strongly on the target q-profile, therefore, making it difficult to evaluate a simple power threshold scaling law as will be discussed further in Section 3. A trigger mechanism for the ITB formation described in the above results has been proposed to be coupling between edge MHD activity (at integer edge q values) and internal integer q surfaces [123], whereby the coupled modes could lead to local changes of the toroidal rotation gradient and subsequent increase in the E×B flow shear. Experimental observations indicate temporal correlation between edge MHD activity and the onset time of ITB formation. Model simulation using a stability code indicate that coupling between internal and edge rational surfaces is possible and consistent with the experimental observation [123]. In the TJ–II stellerator, E×B flow shear has been observed in the proximity of rational surfaces [124]. Also, MHD modes at low order rational surfaces could drive plasma flows through an associated Reynold's stress [125].

2.4. FORMATION AND COMPATIBILITY OF MULTIPLE TRANSPORT BARRIERS

Simultaneous multiple transport barriers, such as a combination of internal transport barriers with an edge transport barrier, have been observed on many machines. However, the dynamics of the formation and co-existence of ITBs with ETBs is dependent on how the various barriers interact with each other to affect the formation conditions for the individual barriers themselves. The combination of ITBs with an ETB is advantageous in that it can: (1) lead to improved performance by increasing the volume of plasma with reduced transport; (2) lead to improved stability against destabilizing ideal n = 1 MHD modes as a result of broadened pressure profiles [126,127]; (3) improve the alignment of the bootstrap current to the total current profile for steady state operation. However, the presence of a strong H–mode edge transport barrier can be very detrimental to the existence of an ITB.

In JET, the strong increase in edge pressure during an ELM-free H–mode ETB degrades the ITB through reduction of the plasma rotation shear and pressure gradient at the ITB location [128]. As also observed in other devices, the large density increase at the plasma edge for an

ETB reduces the effective neutral beam penetration to the plasma core required to form or maintain the ITB. Furthermore, Type I ELM activity leads to an erosion of temperature gradients at the ITB and an inward movement of the ITB [129]. The energy loss from the core then further increases ELM activity eventually leading to a standard ELMy H–mode plasma without an ITB [130]. In order to extend the duration of these so-called double barrier modes, impurity seeding (e.g., argon and krypton) was used to control the edge pressure and modify the current profile by radiation cooling [128]. Subsequently, ITBs were maintained with an H–mode ETB with less obtrusive Type III ELMs. However, the accumulation of impurities in the core leads to a strong dilution of the core plasma and this technique does not provide for a long-term solution. Recently, long duration double barrier mode plasmas have been obtained in JET [131] without impurity seeding by operating at low densities close to the Type III ELM operating densities and maintaining an inferred large current at the plasma edge which prevents the transition from Type III ELMs to Type I ELMs [132].

In ASDEX Upgrade, double barrier modes plasmas combining ITBs with an ELMy H–mode edge have been produced by operating at low density [97]. However, in ASDEX Upgrade, the H–mode ETB is normally avoided with ITBs because the H–mode edge bootstrap current in combination with the large pressure gradients in the ITB lead to the destabilization of external kink modes at rational edge q values [101].

In JT–60U, ITBs can co-exist with the H–mode ETB in the high-β_p H–mode with weak positive magnetic shear [11] and the RS ELMy H–mode with reversed magnetic shear [12]. In fact, the formation of strong ITBs in the JT–60U RS plasmas can inhibit the production of an H–mode barrier because of the reduction in the power flow under the elevated threshold power requirements that will be discussed in Section 3. However, by varying the combination of tangential neutral beams injected into the plasmas, the toroidal rotation was changed resulting in a degradation of the ITB and increased power flow to the plasma edge and the formation of an H–mode ETB [12]. Subsequently, higher values of β_N were achieved with the broadened pressure profiles compared to the ITB with an L–mode edge [12]. This has led to high performance RS plasmas with an ITB in T_i and T_e and an ELMing H–mode edge with values of $\beta_N \sim 1.9$–2.2 and $H_{89} = 3.3$–3.8 for $6\,\tau_E$ [133]. Full noninductive current drive was achieved as a result of a large bootstrap current fraction (~80%) from the ITB and the beam driven current [133].

In DIII–D, the presence of ELMs with an H–mode edge barrier is detrimental to the formation of ITBs [134]. However, the quiescent double barrier (QDB) mode has been produced by combining an ITB with the quiescent H–mode (QH–mode) edge barrier [4,135]. The advantage of the QH–mode edge barrier for the ITB is the absence of ELMs and a low edge density so that the detrimental effects of ELMs on ITBs are avoided and neutral beam penetration to the core is maintained at the low edge density. In fact, the ITB and ETB in the QDB plasmas do not detrimentally affect each other, but rather are additive towards the overall

performance; a $\beta_N H_{89}$ product of 7 has been obtained for 10 τ_E [135], far exceeding product values of 4–5 in normal ELMing H–mode plasmas.

Overall, the formation of simultaneous multiple barriers in plasmas requires satisfying the formation requirements for each barrier, such as: (1) providing good core heating for ITBs (e.g., good neutral beam penetration to the core by maintaining a low edge density in the edge barrier); (2) adequate power flow to the plasma edge for ETB formation (e.g., may require degradation of the ITB to allow energy to flow out); (c) minimizing perturbations that can weaken the barrier (e.g., avoiding Type I ELMs which can penetrate to the plasma core and destroy the ITB).

3. ACCESS CONDITION FOR TRANSPORT BARRIER FORMATION

This section will consider the effects of local conditions on the dynamics and threshold requirements for transport barrier formation. Due to length limitations, a detailed study of threshold requirements will not be given here, but rather the key aspects for barrier formation will be presented.

Clear power thresholds exist for the formation of ITBs and ETBs which have been expressed in the form of global plasma parameters (e.g., B_T, $\bar{n}_e$ etc.) for the H–mode ETB [136] and for ITBs [137,138]. However, transport barrier formation (edge and internal) is very dependent on the local conditions, which can affect the power requirements and the evolution of the barrier. For example in DIII–D, large radiative losses from MARFES located just inside the separatrix and above the divertor X–point produced very slow L–H transitions (~120 ms) than the standard fast ($\lesssim$1 ms) transitions obtained in MARFE-free plasmas [139]. In several machines, changing the divertor geometry has led to changes in the H–mode power threshold, e.g., in JET [140] and JT–60U [141]. More specifically, in JT–60U the reduction in the H–mode power threshold observed with the W–shaped divertor compared to the previous open divertor was explained as the result of the increased edge neutral density at the X–point with the new divertor. In DIII–D, measurements of local neutral densities have indicated the importance of neutrals on the H–mode barrier formation [142] which have shown agreement with theoretical modeling [143]. In some devices the edge T_e has been stressed as being a critical parameter for the formation of the H–mode barrier [144,145]. However, H–mode transitions triggered directly by pellets in DIII–D exhibit a substantial reduction (>50%) in the edge T_e and T_i at the transition as a result of the pellet injection [36] (Fig. 3–1). This is inconsistent with a critical edge temperature controlling the H–mode barrier formation. Also, the power threshold for the H–mode transition was reduced by nearly 30% with pellet injection [36]. It appears that the production of a strong density gradient at the plasma edge by pellet injection facilitates the barrier formation. Furthermore, H–mode transitions triggered directly by pellets allow rigorous tests of H–mode transition theories. The plasma parameters at the pellet triggered H–mode transition are well below the predictions of several transition theories [36].

Whereas edge barrier formation is dependent on the net power loss across the plasma edge, the formation of ITBs is more sensitive to the power deposition profile [72] and, more specifically, deposition inside the radial location of the ITB. This is just one example of how ITB formation conditions differ from those for ETBs: the conditions for ITB formation are very profile-dependent, e.g., the q-profile, the n_e profile, toroidal momentum input profiles, current drive profiles, etc. For example, in JET OS discharges with weak positive central shear, the power threshold for ITB formation was found to scale with B_T [138]. However, in more recent

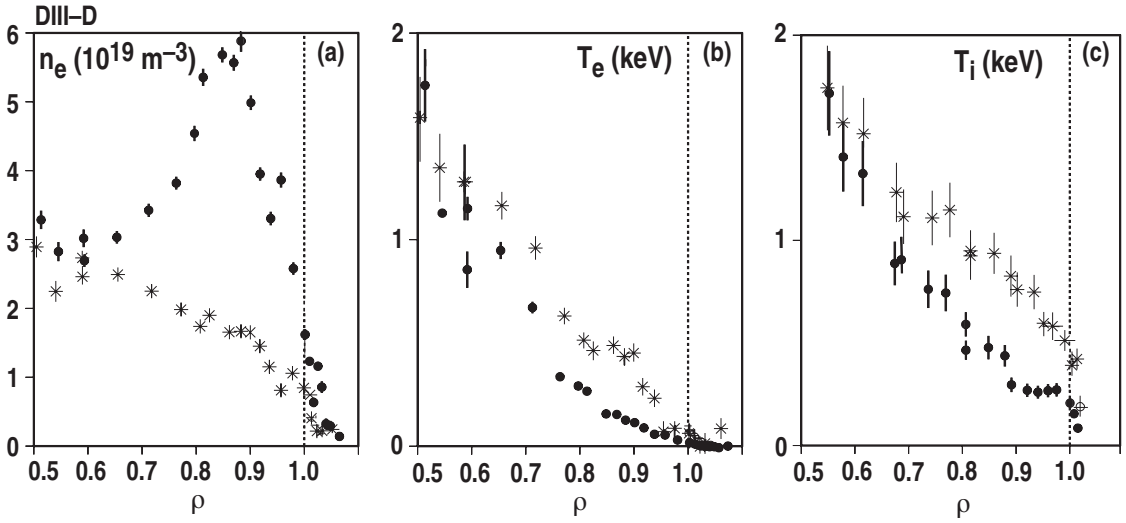

Fig. 3–1. Electron density, electron temperature and ion temperature profiles before and after pellet injection for a pellet-induced H–mode transition in DIII–D. The cross (×) points are before the pellet (18 ms before H–mode transition) and the solid points (●) are just after the pellet injection (6 ms before H–mode transition). The separatrix location is shown by the vertical dashed line. The edge density increases by nearly a factor 4 and the edge temperatures decrease by factor 2–3. The H–mode transition occurred at much reduced power levels (by ~30%) with pellet injection than for reference shots at the same plasma conditions without pellet injection [35].

work with LHCD preheating of the plasma, which produced negative central shear discharges, there is no clear power dependence with B_T [146] as shown in Fig. 3–2. In general, many machines observe that the power requirements for ITB formation are decreased with increased negative central shear. This can be expected from negative central shear reducing the turbulent growth rates and, thereby, facilitating the formation of the ITB. Also, as discussed earlier, electron ITBs are more readily formed in the presence of strong negative central shear and from the stabilizing effect of the Shafranov shift. Therefore, the formation of different types of ITBs (e.g., electron, ion, density, etc.) and locations of ITBs can be affected by tailoring the most favorable combination of profiles (heating, current drive, q, etc.) to achieve the desired barrier characteristics. Note that in some devices, electron ITBs can be formed with LHCD and ECRH at much lower total power than can ion ITBs with neutral beam injection. This is partly related to the highly localized heat deposition afforded by LHCD and ECRH compared to NBI and may also be related to the different threshold requirements for fluctuation suppression of the various modes present in the plasma.

In general, ITB formation is favored by low density operation which aids good neutral beam penetration and or improved coupling of ECH and LH heating and for increased ECCD and LHCD efficiencies. In JT–60U, the threshold power for ITB formation increases strongly with line average density for the positive shear high-β_p mode [137] but has a weak dependence on density for the reversed magnetic shear mode [147] (i.e., negative central shear facilitates ITB

formation). The ITB power threshold also has weak to moderate dependence on density for JET and ASDEX Upgrade [148]. However, again for dominant NBI heating, the threshold power for ITBs can be strongly affected by local variations in the edge density (rather than averaged density), which can be very different for an H–mode edge compared to an L–mode edge.

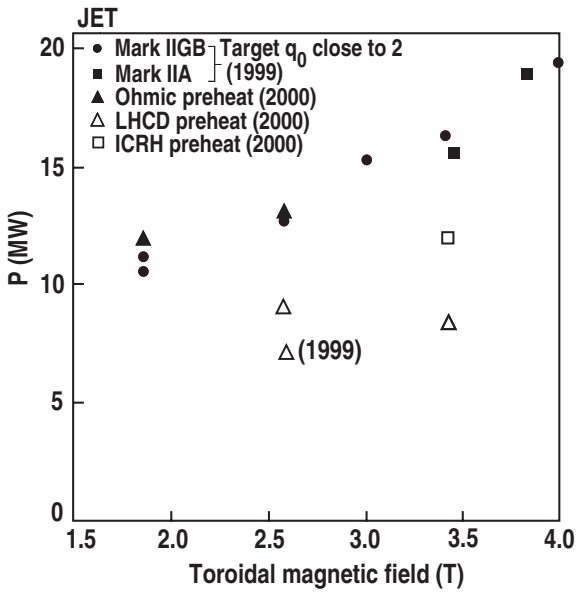

Fig. 3–2. Power threshold for ITB formation as a function of the toroidal magnetic field in JET. The filled symbols represent OS discharges with weak positive central magnetic shear. The open symbols represent discharges with negative central magnetic shear with LHCD preheat producing more negative central shear than ICRH preheat [142].

The threshold power requirements determined from scalings using global parameters can break down for plasmas with multiple barriers. In JT–60U, the threshold power for the H–mode transition is much higher (by factor 2–3) in the presence of strong ITBs than the predicted value from conventional H–mode power scaling [149] as can be seen in Fig. 3–3. Examination of the local edge temperature and density indicates similar values at the H–mode transition with and without strong ITBs, but that the edge density is very low in plasmas with strong ITBs. This then leads to a high H–mode power threshold as observed in conventional H–mode threshold scalings with low density operation. Controlled degradation of the ITB in JT–60U by changing the toroidal momentum input profile using co- and counter-NBI results in an increase in power to the edge [12], but also an increase in the *edge density* which is more favorable for an H–mode transition according to the density scaling. The above results indicate that H–mode threshold power scalings using global parameters are not applicable for plasmas with ITBs because of the variation in the threshold requirements due to the behavior of the local edge conditions.

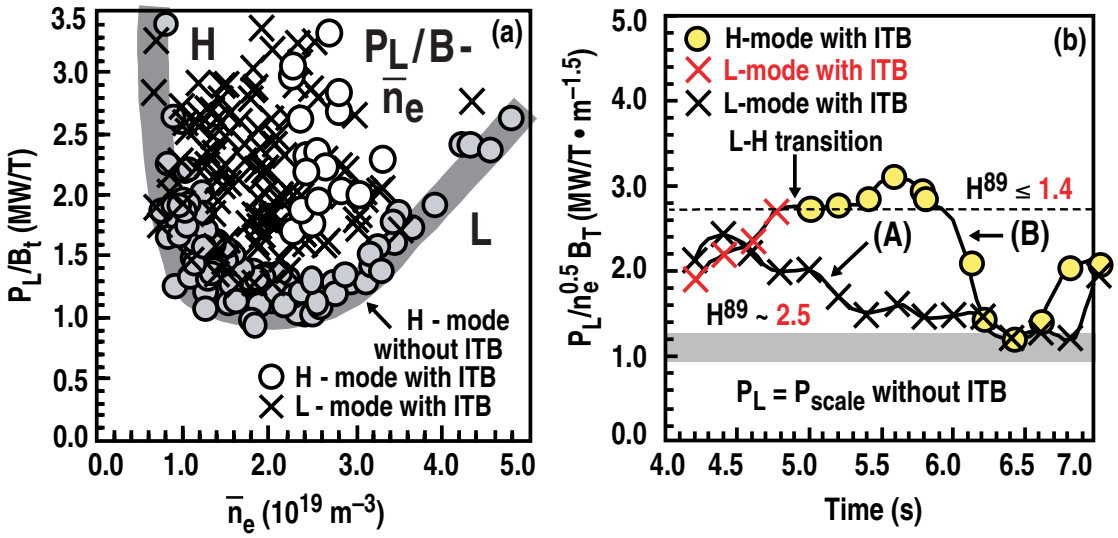

Fig. 3–3. (a) The power required to form the H–mode edge barrier with and without the presence of an ITB in JT–60U (● power for H–mode formation with no ITB, ❍ power for H–mode formation with ITB, × power at which no H–mode barrier was formed with an ITB) (b) time traces of two discharges with ITBs — one discharge exhibited a H–mode transition (❍ points) whilst the other (×) stayed in L–mode. Also shown is the L–H threshold power from the scaling law for the H–mode threshold without ITBs [145].

4. DESTRUCTION OF TRANSPORT BARRIERS

The reduced transport and high plasma confinement achieved through transport barriers generate large pressure gradients P′ which can drive MHD instabilities that often degrade or destroy the barrier. For edge transport barriers, these instabilities manifest themselves as ELMs which are repeating cycles of destruction and reformation of the edge barrier. ELMs can be beneficial to the longevity of the H–mode edge barrier in that the periodic degradation of the barrier helps to control the increase of density and impurities in the plasma, otherwise the barrier would be irreversibly destroyed through excessive radiative power loss. Due to space constraints, a detailed description of the MHD instability properties of the ELMs will not be presented (see, e.g., reviews of ELMs [67,150]). In fact, the H–mode edge barrier can persist well (albeit degraded depending on the ELM type) in the presence of ELMs, rather it is the effects that the ELMs have on other items, such as, the divertor surfaces that can make them detrimental. Type I ELMs can also destroy ITBs as noted earlier [129,134]. Operationally, the H–mode edge barrier is destroyed (reverts back to L–mode confinement) at high densities (the H–mode density limit) [151–153].

In the case of the plasma core, ITBs are not only destroyed by Type I ELMs, they can be degraded and destroyed through power starvation resulting from the high edge densities and pressure associated with the H–mode edge barrier [128]. However, the ITBs are fundamentally limited by pressure driven ideal MHD instabilities as a result of the large values of P′ and pressure peaking associated with the barrier. In JET, disruption in ITB discharges at relatively low β_N have been associated with the n = 1 pressure driven kink mode [154]. Disruption can be avoided with less peaked pressure profiles, but then "snakes" may appear [155], which are nonlinear magnetic perturbations associated with the q = 2 surface and have a radial extent of ~10 cm near the foot of the ITB. In JT–60U and DIII–D, n = 1 ideal MHD instabilities with very peaked pressure profiles (with L–mode edge) also lead to ITB collapse [156,157]. In DIII–D, resistive interchange modes are destabilized in the negative shear region [158]. In JT–60U, ITBs formed in negative central shear plasmas suffered from major disruptions when q_{min} passed through simple rational values [12]. In ASDEX, disruptive termination of the ITB occur just after an H–mode transition when a pressure-driven ideal mode couples to an external kink when q_{95} is near a simple rational value [159].

The n = 1 instabilities can be avoided by decreasing the pressure profile peakedness, as predicted by ideal stability theory [160,161]. However, with broader pressure profiles, stability limitations due to neoclassical tearing modes may then occur [162]. Clearly, plasma stability becomes a key issue given the low level of transport and the improved confinement produced by transport barriers. The issues of transport reduction and plasma stability have to be treated in unison to achieve effective steady state, high performance plasma operation.

5. CONTROL OF TRANSPORT BARRIERS

To achieve high plasma stability and high confinement, there is an important need to develop tools for the dynamic control of transport barrier (e.g., strength, duration, location). Fundamentally, this requires control of the plasma profiles, such as the plasma pressure, rotation, and current profiles.

The increased understanding of transport barrier formation through E×B velocity shear stabilization of turbulence has provided methods to control transport barriers by changing the E×B shearing rate by, for example, changes in the toroidal plasma rotation. In tests of causality in DIII–D, magnetic braking in VH–mode discharges and high ℓ_i discharges was used to change the toroidal plasma rotation, v_ϕ, and, hence, the E×B shearing rate resulting in clear changes to the plasma transport [64,65]. Similarly in TFTR, changes in the mix of co-injected and counter-injected neutral beams (and toroidal rotation) during the steady state ERS phase led to significant charges in the E×B shearing which then directly led to changes in the plasma transport [73]. In JT–60U, changes in the NBI toroidal momentum input have been used to alter v_ϕ and E_r and, thereby, control the T_i gradient at the ITB [163].

In the case of the edge transport barrier, the edge pedestal characteristics (and ELM behavior) can be affected by plasma shaping {e.g., by triangularity and elongation in JT–60U [164], by triangularity in ASDEX Upgrade [165], by triangularity and squareness in DIII–D [166,167] by impurity gas seeding (e.g., in JET [128]) and by pellet injection (in DIII–D [167])}.

Ultimately, it is *real-time control* of the plasma profiles that is required for steady state operation with ITBs. In JT–60U, the plasma β was controlled in real time by feedback of the neutron emission rate onto the neutral beam power [12]. In this manner, the major disruptions that normally occurred at the passing of $q_{min} = 3$ were avoided. More recently in JT–60U, the strength of the ITB was controlled by feedback of the diamagnetic stored energy on the perpendicular neutral beam power [163]. The ITB was intentionally degraded using co-injected NBI after its initial formation with nearly balanced beams. On ITB degradation, real-time feedback of the perpendicular NB power was applied to restore the ITB as shown in Fig. 5–1. The perpendicular NB did not introduce any significant toroidal momentum torque in the plasma. The shear in the E_r profile is low on ITB degradation, but has significantly increased on ITB reformation and was able to sustain the ITB even with a much reduced heating power for about 1 s.

In JET, real-time control of the electron temperature profile (and, thereby, the electron ITB) in plasmas with simultaneous electron and ion ITBs has been achieved using the output from the 48-channel ECE diagnostic system fed back to the ICRH power [168]. In JET, electron ITBs can be characterized by a local dimensionless parameter, $\rho^*_{T_e} = \rho_s/L_{T_e}$ where ρ_s is the local Larmor

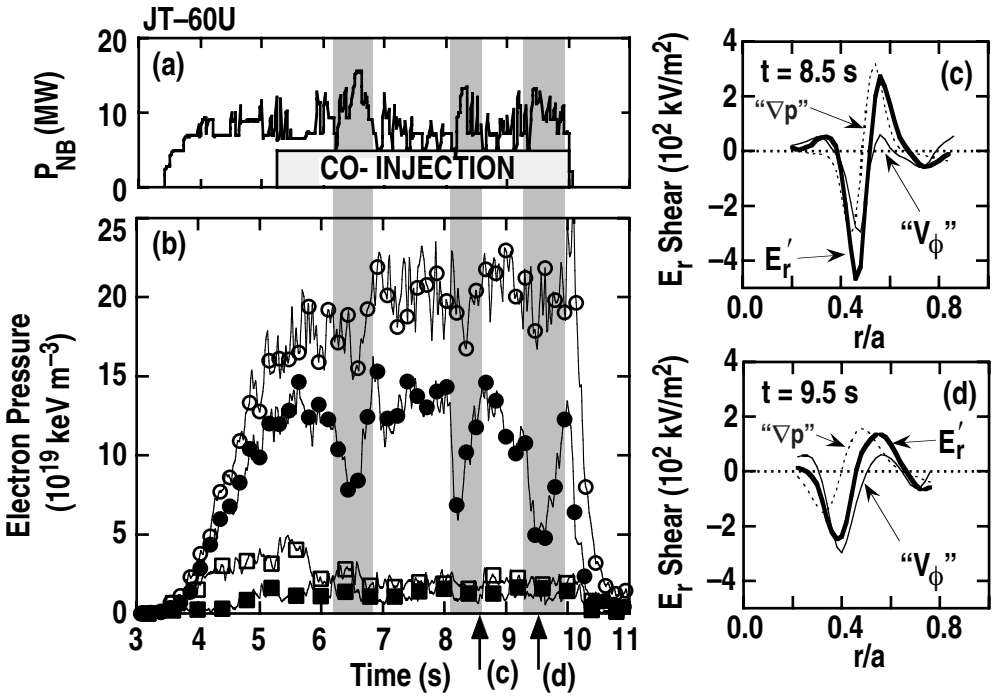

Fig. 5–1. (a) Waveform of NB power showing time of dominant co-NB power. (b) Time traces of the electron pressure at various radial locations (r/a = 0.3 ○, r/a = 0.5 ●, r/a = 0.7 ❑, r/a = 0.9 ■). (c) Profiles of the E_r shear and the contribution from ∇P and v_ϕ at t = 8.5 s (strong ITB phase). (d) Profiles of E_r shear and its components at t = 9.5 s (weak ITB phase) [159].

radius at the ion sound speed and L_{T_e} is the electron temperature gradient scale length $L_{T_e} = -T_e/(\partial T_e/\partial r)$ [169]. An ITB exists if $\rho^*_{T_e} \gtrsim 0.014$ as determined from statistical analysis of a large database of JET discharges. Using the 48 channels of the ECE heterodyne radiometer, the electron temperature profile was fed back to the ICRH power for real time control of the ITB at a chosen value of $\rho^*_{T_e} = 0.025$ [168]. Furthermore, steady state high performance discharges were achieved by using a double feedback algorithm to separately control the neutron rate (with NBI) and the temperature gradient (with ICRH). Figure 5–2 shows control of the ITB for nearly 7.5 s with $\rho^*_{T_e}$ and the neutron rate maintained at near constant values of 0.025 and 9×10^{15} neutron s^{-1}, respectively. An uncontrolled discharge is shown in comparison, which suffers from MHD limitations as can be seen in the time history of the $\rho^*_{T_e}$ plot signifying collapses in the ITB. The controlled discharge had slightly reduced performance, but had much better stability. The real time control system is now being applied to produce steady state high performance plasmas in JET with full current drive operation. (Note that the loop voltage in Fig. 5–2 is close to zero.) [170].

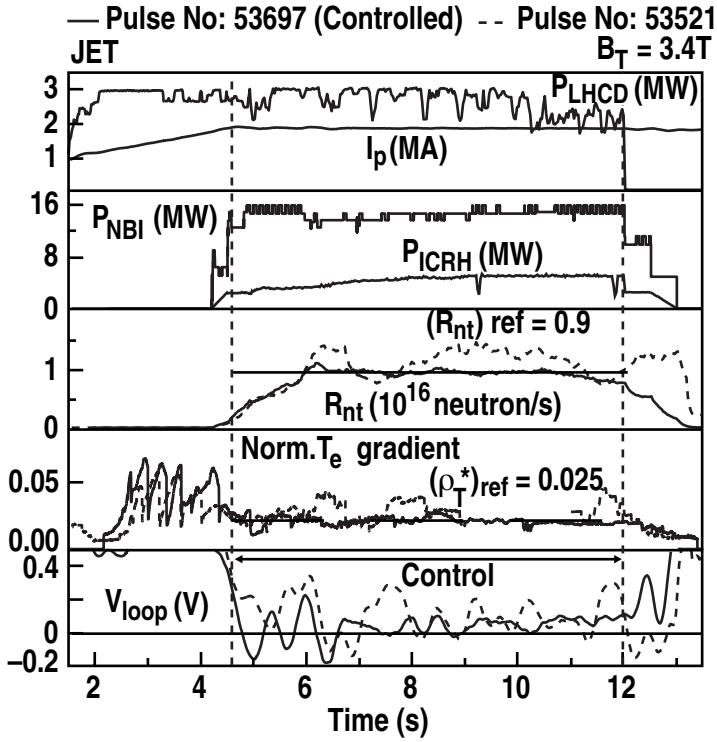

Fig. 5–2. Time traces of a JET discharge showing real time control of the ITB and the neutron rate (solid trace) with ICRH and NBI, respectively. Control is maintained from 4.5 s for 7.5 s. The ITB control parameter, $\rho^{\sim}_{T_e}$, is maingtained at a value of 0.025 and the neutron rate, R_{nt}, is maintained at 0.9×10^{16} neutron s^{-1}. The loop voltage is close to zero. A comparison shot without feedback control (dashed trace) exhibits collapses due to MHD limits [164].

6. SUMMARY

A good understanding of transport barrier formation has been achieved through examination of mechanisms that can stabilize plasma turbulence and, thereby, reduce turbulence-driven transport. Stabilization of turbulence of E×B velocity shear has been observed to be related to barrier formation in many devices and under a wide range of conditions. Tests of causality have shown that E×B velocity shear directly affects transport in barriers located anywhere from the plasma edge to the plasma core (e.g., H–mode, VH–mode and ITBs). Consequently, tools have been developed to control barriers by changing the E×B shearing rate, such as, by changing the momentum input to the plasma. For internal transport barriers, the effectiveness of E×B velocity shear stabilization is facilitated by negative central magnetic shear and the Shafranov shift. However, negative central magnetic shear is neither a necessary nor sufficient condition for ion, momentum and particle ITBs and even, in some cases, electron ITBs. Ion transport in ITBs can be reduced to neoclassical levels, but electron transport usually remains anomalously high. However, significant reduction in electron transport is more prevalent in plasmas with negative central shear. This has been observed most clearly in Tore Supra where there was a significant correlation between reduced core electron transport and increased negative central shear. In DIII–D, the reduction in electron transport in the electron ITB is attributed to α-stabilization of the ETG modes. E×B velocity shear is considered less effective for stabilization of ETG modes because of the smaller spatial scales involved. However, electron ITBs can also be generated in plasmas with positive magnetic shear as observed in TUMAN–3M and JT–60U and α-stabilization is normally considered to be destabilizing in positive magnetic shear.

Understanding processes that can generate spontaneous perpendicular flow in plasmas is an important issue. In ASDEX Upgrade, the formation of ITBs after the onset of fishbone activity is attributed to the generation of sheared flow resulting from the interaction between fishbones and the resonant fast particle from the neutral beams. Also, observation of bicoherence between fluctuations at different spatial scales just before the H–mode transition in DIII–D is considered to be consistent with a transient Reynold's stress driven zonal flow shear. The observations on some devices that link the formation of ITBs with rational q surfaces is being explained through mechanisms that may generate E×B flow at these surfaces.

Clear thresholds exist for the formation of transport barriers. However, these thresholds are very dependent on local quantities rather than on global parameters. Furthermore, for ITBs, the barrier formation dynamics are very profile dependent (e.g., power deposition profile, q profile, input momentum profile, etc.). Increased negative central shear tends to lower the threshold power requirements for ITB formation. In JET, the power threshold dependence on B_T observed in OS (weak positive shear) discharges is just about nullified in negative magnetic shear

discharges produced by LHCD preheat. This emphasizes again that barrier formation is dependent on local conditions rather than on global parameters. For the H–mode transport barrier, the edge temperature has been considered to be a critical quantity for barrier formation. However, pellet triggered H–modes in which the edge temperature is substantially reduced at the H–mode transition is inconsistent with the barrier formation being dependent on a critical edge temperature. The power threshold scalings developed using global parameters break down for plasmas with multiple barriers. This is because the various barriers affect the energy flow to each other as well as the formation conditions for the barriers. In JT–60U, the threshold power for the H–mode transition is much higher in the presence of strong ITBs than the predicted value from conventional H–mode power scalings.

For high plasma performance with good plasma stability, real-time control of transport barriers is required through control of the plasma profiles. Real-time control of electron ITBs has been demonstrated at JET. Methods and tools have to be further developed which utilize our improved understanding of barrier formation and subsequent evolution to control transport at the desired level and which is stable to MHD instabilities for effective steady state operation.

7. ACKNOWLEDGEMENTS

This work was supported by the U.S. Department of Energy under Contract No. DE-AC03-99ER54463. The author would like to thank the following people for providing material for this paper: A. Becoulet, K.H. Burrell, T.N. Carlstrom, S. Coda, G.D. Conway, E.J. Doyle, A. Fujisawa, T. Fujita, T. Fukuda, C.M. Greenfield, R.J. Groebner, S. Gunter, Y. Kamada, J.E. Kinsey, L.L. Lao, X. Litaudon, Y. Miura, R.A. Moyer, M. Murakami, A.G. Peeters, J.E. Rice, Y. Sakamoto, A. Sips, G.M. Staebler, R.C. Wolf.

8. REFERENCES

[1] Wagner F et al 1982 *Phys. Rev. Lett.* **49** 1408

[2] Jackson G L et al 1991 *Phys. Rev. Lett.* **67** 3098

[3] Greenwald M et al 1999 *Phys. Plasmas* **6** 1943

[4] Burrell K H et al 2001 *Phys. Plasmas* **8** 2153

[5] Strait E J et al 1995 *Phys. Rev. Lett.* **75** 4421

[6] Levinton F M et al 1995 *Phys. Rev. Lett.* **75** 4417

[7] Koide Y et al 1994 *Phys. Rev. Lett.* **72** 3662

[8] Sips A C et al 1997 *Plasma Phys. Control. Fusion* **40** 647

[9] Greenfield C M et al 2001 *Phys. Rev. Lett.* **86** 4544

[10] Soldner F X et al 1998 *Nucl Fusion* **39** 1883

[11] Kamada Y et al 1999 *Nucl Fusion* **39** 1845

[12] Fujita T et al 1999 *Nucl. Fusion* **39** 1627

[13] Biglari H et al 1990 *Phys. Fluids B* **2** 1

[14] Shaing K C et al 1990 *Phys. Fluids B* **2** 1492.

[15] Itoh K and Itoh S-I 1996 *Plasma Phys. Control. Fusion* **38** 1

[16] Waltz R E et al 1995 *Phys. Plasmas* **2** 2408

[17] Wang X H et al 1992 *Phys. Fluids B* **4** 2402

[18] Beer M A et al 1997 *Phys. Plasmas* **4** 1792

[19] Drake J F et al 1996 *Phys. Rev. Lett.* **77** 494

[20] Dominquez R R and Staebler G M 1993 *Nucl. Fusion* **33** 51

[21] Fröjdg M et al 1992 *Nucl. Fusion* **32** 419

[22] Kotschenreuther M et al 1995 *Phys. Plasmas* **2** 2381

[23] Waltz R E et al 1994 *Phys. Plasmas* **1** 2229

[24] Dorland W et al 2000 *Phys. Rev. Lett.* **85** 5579

[25] Itoh S I and Itoh K 1988 *Phys. Rev. Lett.* **60** 2276

[26] Shaing K C and Crume E C 1989 *Phys. Rev. Lett.* **63** 2369

[27] Hahm T S and Burrell K H 1995 *Phys. Plasmas* **2** 1648

[28] Lohr J et al 1988 *Phys. Rev. Lett.* **60** 2630

[29] Tsuji S et al 1990 *Phys. Rev. Lett.* **64** 1023

[30] Steinmetz K et al 1987 *Phys. Rev. Lett.* **58** 124

[31] Osborne T H et al 1990 *Nucl. Fusion* **30** 2023

[32] Taylor R J et al 1989 *Phys. Rev. Lett.* **63** 2365

[33] Weynants R R et al 1998 *Plasma Phys. Control. Fusion* **40** 635

[34] Jachmich S et al 1998 *Plasma Phys. Control. Fusion* **40** 1105

[35] Askinazi L G et al 1993 *Phys. Fluids B* **5** 2420

[36] Gohil P et al 2001 *Phys. Rev. Lett.* **86** 644

[37] Gohil P et al 1998 *Nucl. Fusion* **38** 93

[38] Burrell K H et al 1995 *Proc. Fifteenth Int. Conf. on Plasma Physics and Controlled Fusion* (Vienna: International Atomic Energy Agency) Vol 1 p 221

[39] Moyer R et al 1995 *Phys. Plasmas* **2** 2397

[40] Moyer R A et al 1999 *Plasma Phys. Control. Fusion* **41** 243

[41] Gohil P et al 1994 *Nucl. Fusion* **34** 1057

[42] Coda S et al 2000 *Phys. Lett. A* **273** 125

[43] Ida K et al 1990 *Phys. Rev. Lett.* **65** 1364

[44] Field A R et al 1992 *Nucl. Fusion* **32** 1191

[45] Wagner F et al 1994 *Plasma Phys. Control. Fusion* **36** A61

[46] Carolan P et al 2001 presented at the *Twenty-eighth European Conf. on Controlled Fusion and Plasma Physics*

[47] Ido T et al 2000 *Plasma Phys. Control. Fusion* **42** A307

[48] Rudakov D L et al 2001 *Plasma Phys. Control. Fusion* **43** 559

[49] Burrell K H et al 1999 *Phys. Plasmas* **6** 441

[50] Hassam A B et al 1991 *Phys. Rev. Lett.* **66** 309

[51] Diamond P H and Kim Y-B 1991 *Phys. Fluids* **3** 1626

[52] Lin Z et al 1998 *Science* **281** 1835

[53] Kim J et al 1994 *Phys. Rev. Lett.* **72** 2199

[54] Moyer R et al 2001 *Phys. Rev. Lett.* to be published

[55] Tynan G R et al 2001 submitted to *Phys. Plasmas*

[56] Diamond P H et al 2000 *Proc. Eighteenth IAEA Fusion Energy Conf.* to be published

[57] Carlstrom T N et al 1999 *Nucl. Fusion* **39** 1941

[58] Carlstrom T N et al 2001 presented at *Eighth IAEA Tech. Committee Mtg. on H-mode Physics and Transport Barriers Physics*

[59] Greenfield C M 1993 *Plasma Phys. Control. Fusion* **35** B263

[60] Burrell K H et al 1993 *Proc. Twentieth European Conf. on Controlled Fusion and Plasma Physics* (Petit-Lancy: European Physical Society) Vol 17C p 27

[61] Rettig C L et al 1993 *Phys. Fluids B* **5** 2428

[62] Osborne T H et al 1995 *Nucl. Fusion* **35** 23

[63] La Haye R J et al 1993 *Nucl. Fusion* **33** 349

[64] La Haye R J et al 1995 *Nucl. Fusion* **35** 988

[65] Lao L L 1998 *Phys. Plasmas* **5** 1050

[66] Zohm H 1996 *Plasma Phys. Control. Fusion* **38** 105

[67] Lao L L et al 2000 *Plasma Phys. Control. Fusion* **42** A51

[68] Burrell K H 1999 *Bull. Am. Phys. Soc.* **44** 127

[69] Hubbard A et al 2001 *Phys. Plasmas* **8** 2033

[70] Kamada Y et al 2000 *Plasma Phys. Control. Fusion* **42** A247

[71] Doyle E J et al 2001 presented at the *Twenty-eighth European Conf. on Controlled Fusion and Plasma Physics*

[72] Koide Y et al 1995 *Plasma Phys. and Control. Nucl. Fusion Research* (Vienna: International Atomic Energy Agency) Vol 1 p 199

[73] Synakowski E J 1997 *Phys. Plasmas* **4** 1736

[74] Litaudon X et al 2001 *Plasma Phys. Control. Fusion* **43** 677

[75] Fujita T et al 1998 *Nucl. Fusion* **38** 207

[76] Burrell K H 1997 *Phys. Plasmas* **4** 1499

[77] Diamond P H 1997 *Phys. Rev. Lett.* **78** 1472

[78] Mazzucato E et al 1996 *Phys. Rev. Lett.* **77** 3145

[79] Rettig C L et al 1998 *Phys. Plasmas* **5** 1727

[80] Newman D E et al 1998 *Phys. Plasmas* **5** 938

[81] Conway G D et al 2000 *Phys. Rev. Lett.* **84** 1463

[82] Burrell K H 1998 *Plasma Phys. Control. Fusion* **40** 1589

[83] Lazarus E A et al 1996 *Phys. Rev. Lett.* **77** 2714

[84] Doyle E J et al 1997 *Proc. Sixteenth IAEA Fusion Energy Conf.* (Vienna: International Atomic Energy Agency) Vol 1 p 547

[85] Schissel D P et al 1997 *Proc. Sixteenth IAEA Fusion Energy Conf.* (Vienna: International Atomic Energy Agency) Vol 1 p 463

[86] Esposito B et al 2001 presented at the *Twenty-eighth European Conf. on Controlled Fusion and Plasma Physics*

[87] Crisanti F et al 2001 *Nucl. Fusion* **41** 883

[88] McKee G R et al 2000 *Phys. Plasmas* **7** 1870

[89] Murakami M et al 2000 *Proc. Eighteenth IAEA Fusion Energy Conf.* to be published

[90] Waltz R E et al 1997 *Phys. Plasmas* **4** 2482

[91] Hammett G et al 1990 *Phys. Rev. Lett.* **64** 3019

[92] Kishimoto Y et al 1997 *Proc. Sixteenth International Conf. on Plasma Physics and Controlled Nuclear Fusion Research* (Vienna, International Atomic Energy Agency) Vol 2 p 581

[93] Garbet X et al 2001 *Phys. Plasmas* **8** 2023

[94] Fujisawa A 1999 *Phys. Rev. Lett.* **82** 2669

[95] Staebler G M et al 2001 *Nucl. Fusion* **41** 891

[96] Gunter S et al 2001 presented at the *Twenty-eighth European Conf. on Controlled Fusion and Plasma Physics*

[97] Wolf R et al 1999 *Plasma Phys. Control. Fusion* **41** B93

[98] Pinches S D et al 2001 presented at the *Twenty-eighth European Conf. on Controlled Fusion and Plasma Physics*

[99] Doyle E J et al 2000 *Plasma Phys. Control. Fusion* **42** A236

[100] Baranov Y et al 1999 *Proc. Twenty-sixth European Conf. on Controlled Fusion and Plasma Physics* (Petit-Lancy: European Physical Society) Vol 23J p 169

[101] Wolf R et al 2000 *Proc. Eighteenth IAEA Fusion Energy Conf.* to be published

[102] Equipe Tore Supra 1996 *Plasma Phys. Control. Fusion* **38** A251

[103] Hoang G T et al 2000 *Phys. Rev. Lett.* **84** 4593

[104] Hogeweij G M D et al 2001 presented at the *Twenty-eighth European Conf. on Controlled Fusion and Plasma Physics*

[105] Greenfield C M et al 2000 *Proc. Twenty-seventh European Conf. on Controlled Fusion and Plasma Physics* (Budapest: European Physical Society) Vol 24B p 544

[106] Buratti P et al 1999 *Phys. Rev. Lett.* **82** 560

[107] Pietrzyk Z A et al 2000 *Phys. Plasmas* **7** 2909

[108] Lopes-Cardozo L et al 1997 *Plasma Phys. Control. Fusion* **39** B303

[109] LeBlanc B et al 1995 *Phys. Plasmas* **2** 741

[110] Cesario R 2001 submitted to *Phys. Rev. Lett.*

[111] Rice J E et al 2001 *Nucl. Fusion* **41** 277

[112] Jenko F et al 2000 *Phys. Plasmas* **7** 1904

[113] Stallard B W et al 1999 *Phys. Plasmas* **6** 1978

[114] Waltz R E et al 1999 *Phys. Plasmas* **6** 4265

[115] Peeters A G et al 2000 *Proc. Eighteenth IAEA Fusion Energy Conf.* to be published IAEA-CN-77/EXP5/06

[116] Lebedev S V et al 1998 *Plasma Phys. Control. Fusion* **40** 741

[117] Bell R E et al 1998 *Plasma Phys. Control. Fusion* **40** 609

[118] de Baar M R et al 1997 *Phys. Rev. Lett.* **78** 4573

[119] Koide Y et al 1994 *Plasma Phys. Control. Fusion* **36** A195

[120] Kamada Y et al 1992 *Phys. Fluids B* **4** 124

[121] Challis C D et al 1999 *Proc. Twenty-sixth European Conf. on Controlled Fusion and Plasma Physics* (Nieuwegein: European Physical Society) Vol 23J p 69

[122] Joffrin E et al 2001 presented at the *Twenty-eighth European Conf. on Controlled Fusion and Plasma Physics*

[123] Joffrin E et al 2000 *Proc. Twenty-seventh European Conf. on Controlled Fusion and Plasma Physics* (Budapest: European Physical Society) Vol 24B p 237

[124] Pedrosa M A et al 1999 presented at the *Twenty-sixth European Conf. on Controlled Fusion and Plasma Physics* (Nieuwegein: European Physical Society) Vol 23J p 377

[125] Thyagaraja A 2000 *Plasma Phys. Control. Fusion* **42** B255

[126] Lao L L et al 1996 *Phys. Plasmas* **3** 1951

[127] Turnbull A D 1998 *Nucl. Fusion* **38** 1467

[128] Sips A C C et al 2000 *Proc. Eighteenth IAEA Fusion Energy Conf.* to be published

[129] Sarazin Y et al 2000 *Proc. Twenty-seventh European Conf. on Controlled Fusion and Plasma Physics* (Budapest: European Physical Society) Vol 24B p 253

[130] Soldner F X et al 1997 *Plasma Phys. Control. Fusion* **39** B353

[131] Litaudon X et al 2001 presented at the *Twenty-eighth European Conf. on Controlled Fusion and Plasma Physics*

[132] Becoulet M et al 2001 presented at the *Twenty-eighth European Conf. on Controlled Fusion and Plasma Physics*

[133] Fujita T et al 2001 *Phys. Rev. Lett.* **87**

[134] Rice B W et al 1999 *Nucl. Fusion* **39** 1855

[135] Doyle E J et al 2001 presented at the *Twenty-eighth European Conf. on Controlled Fusion and Plasma Physics*

[136] Ryter F et al 1996 *Nucl. Fusion* **36** 1217

[137] Koide Y et al 1996 *Plasma Phys. Control. Fusion* **38** 1011

[138] Gormezano C et al 1999 *Special Issue of Nucl. Fusion* (*Seventeenth IAEA Fusion Energy Conf.*) **39** 2015

[139] Moyer R A et al 1999 *Plasma Phys. Control. Fusion* **41** 243

[140] Horton L D et al 1999 *Proc. Twenty-sixth European Conf. on Controlled Fusion and Plasma Physics* (Nieuwegein: European Physical Society) Vol 23J p 193

[141] Tsuchiya K et al 2000 *Proc. Eighteenth IAEA Fusion Energy Conf.* to be published

[142] Colchin R J et al 2000 *Nucl. Fusion* **40** 175

[143] Carreras B A 1998 *Phys. Plasmas* **5** 2623

[144] Hubbard A et al 1998 *Plasma Phys. Control. Fusion* **40** 689

[145] Ryter F et al 1998 *Plasma Phys Control. Fusion* **40** 725

[146] Becoulet A 2001 presented at the *Twenty-eighth European Conf. on Controlled Fusion and Plasma Physics*

[147] Kamada Y 1999 *Plasma Phys. Control. Fusion* **42** A65

[148] Fukuda T et al 2001 presented at the *Twenty-eighth European Conf. on Controlled Fusion and Plasma Physics*

[149] Fukuda T et al 2001 presented at *Eighth IAEA Tech. Committee Mtg. on H-mode Physics and Transport Barriers Physics*

[150] Suttrop W 2000 *Plasma Phys. Control. Fusion* **42** A1

[151] Petrie T et al 1993 *Nucl. Fusion* **33** 929

[152] Horton L D et al 1996 *Plasma Phys. Control. Fusion* **38** A269

[153] Mertens V et al 1999 *Proc. Twenty-sixth European Conf. on Controlled Fusion and Plasma Physics* (Petit-Lancy: European Physical Society) Vol 23J p 1397

[154] Huysman G T A 1999 *Nucl. Fusion* **39** 1489

[155] Alper B 1999 *Proc. Twenty-sixth European Conf. on Controlled Fusion and Plasma Physics* (Petit-Lancy: European Physical Society) Vol 23J p 173

[156] Ishida T et al 1997 *Proc. Twenty-fourth European Conf. on Controlled Fusion and Plasma Physics* (European Physical Society) Vol 21A Part 2 p 489

[157] Strait E J et al 1997 *Phys. Plasmas* **4** 1783

[158] Chu M S et al 1996 *Phys. Rev. Lett.* **77** 2710

[159] Gunter S et al 2000 *Nucl. Fusion* **40** 1541

[160] Lao L L et al 1996 *Phys. Plasma* **3** 1951

[161] Turnbull A D 1998 *Nucl. Fusion* **38** 1467

[162] Sauter O et al 1997 *Phys. Plasmas* **4** 1654

[163] Sakamoto Y 2000 *Proc. Eighteenth IAEA Fusion Energy Conf.* to be published

[164] Kamada Y et al 1999 *Plasma Phys. Control. Fusion* **41** 1371

[165] Suttrop W et al 2000 *Plasma Phys. Control. Fusion* **42** A97

[166] Osborne T H et al 2000 *Plasma Physics and Control. Fusion* **42** A175

[167] Ferron J R et al 2000 *Proc. Twenty-seventh European Conf. on Controlled Fusion and Plasma Physics* (Budapest: European Physical Society) Vol 24B p 548

[168] Mazon D et al 2001 presented at the *Twenty-eighth European Conf. on Controlled Fusion and Plasma Physics*

[169] Tresset G et al 2001 presented at the *Twenty-eighth European Conf. on Controlled Fusion and Plasma Physics*

[170] Litaudon X et al 2001 presented at the *Twenty-eighth European Conf. on Controlled Fusion and Plasma Physics*